Quantum interference of resonance fluorescence from Germanium-vacancy color centers in diamond

Disheng Chen, †,‡ Johannes E. Fröch, ¶ Shihao Ru, $^{\dagger,\$}$ Hongbing Cai, †,‡ Naizhou Wang, †,‡ Giorgio Adamo, ‡ John Scott, $^{\P,\parallel}$ Fuli Li, § Nikolay Zheludev, $^{\dagger,\ddagger,\perp}$ Igor Aharonovich, $^{*,\P,\parallel}$ and Wei-bo Gao *,†,‡

†Division of Physics and Applied Physics, School of Physical and Mathematical Sciences,

Nanyang Technological University, Singapore 637371, Singapore

‡The Photonics Institute and Centre for Disruptive Photonic Technologies, Nanyang

Technological University, Singapore 637371, Singapore

¶School of Mathematical and Physical Sciences, University of Technology Sydney, Ultimo,

NSW, 2007, Australia

§Shaanxi Key Laboratory of Quantum Information and Quantum Optoelectronic Devices,

School of Physics, Xi'an Jiaotong University, Xi'an 710049, China

||ARC Centre of Excellence for Transformative Meta-Optical Systems (TMOS), Faculty of

Science, University of Technology Sydney, Ultimo, New South Wales 2007, Australia

⊥Optoelectronics Research Centre, University of Southampton, Hampshire, SO17 1BJ, UK

E-mail: igor.aharonovich@uts.edu.au; wbgao@ntu.edu.sg

Abstract

Resonance fluorescence from a quantum emitter is an ideal source to extract indistinguishable photons. By using the cross polarization to suppress the laser scattering, we observed resonance fluorescence from GeV color centers in diamond at cryogenic temperature. The Fourier-transform-limited linewidth emission with $T_2/2T_1 \sim 0.86$ allows for two-photon interference based on single GeV color center. Under pulsed excitation, the 24 ns separated photons exhibit a Hong-Ou-Mandel visibility of 0.604 ± 0.022 , while the continuous-wave excitation leads to a coalescence time window of 1.05 radiative lifetime. Together with single-shot readout of spin states, it paves the way towards building a quantum network with GeV color centers in diamond.

Key words: Germanium vacancy color center in diamond, resonance fluorescence, two-photon interference, single-shot readout

Indistinguishable photons are indispensable resources for photonic quantum information processing¹ and underlie several key quantum technologies including linear optical quantum computing,² remote quantum-state teleportation,³ and quantum-repeater-enabled large-scale quantum network.⁴ Various optical processes or single-photon emitters have been explored to generate these identical photons, such as non-linear down-conversion process,⁵ single atoms⁶ or ions,⁷ semiconductor quantum dots,⁸ and solid-state quantum emitters.⁹ The latter stands out for the spin-tagged photonic interface,¹⁰ mature nanostructure fabrications,¹¹ and the potential to scale up with the quantum photonic integrated circuits.^{12,13}

The negatively charged Germanium vacancy (GeV⁻) color center in diamond exhibits a stable spectrum with negligible inhomogeneous broadening ¹⁴ thanks to the inversion-symmetry of its D_{3d} molecular structure, ¹⁵ which effectively suppresses the first-order response to the electric-field jittering. ¹⁶ Together with the high quantum efficiency of radiative decay (30%) ¹⁷ and large zero-phonon line (ZPL) proportion (70%), ¹⁸ GeV color center may present a unique opportunity, similar to that of Silicon vacancy (SiV) color center, to realize solid-state quantum nodes without invoking any frequency-tuning technique. ¹⁹ Both GeV and SiV color centers feature superior optical properties compared to NV centers in diamond by sparing some of their spin coherence time. In addition, the GeV exhibits 3 times higher radiative decay rate than SiV, which not only yields stronger single photon emission inten-

sity, it also provides more fault-tolerance rooms when integrating these quantum emitters in nanophotonic devices.

Here, we show that the presence of a microstructure around the GeV does not impair its optical properties and the lifetime-limited linewidth emission can be observed. This narrow linewidth allows for two-photon interference (TPI) based on indistinguishable photons from a single GeV emitter with a Hong-Ou-Mandel (HOM) effect. ²⁰ Together with the single-shot readout of GeV spin state enabled by enhanced photon collection efficiency using a solid immersion lens, this paves the road towards high-fidelity, high-rate spin-photon entanglement based on solid-state quantum emitters.

The GeV color centers in this work are generated via high-energy ion implantation (10 MeV, 10^{10} cm²) on a Type-IIa diamond substrate, followed by high-temperature high-vacuum annealing 21,22 that helps GeV formation and lattice repair (details in Supporting Information 23). Before implantation, an array of solid immersion lens (SIL) is fabricated on the surface of the diamond via focused ion beam (FIB) milling, which provides a $3 \sim 8$ times boost in the photoluminescence (PL) collection efficiency as compared to the flat surface. 24,25 Acid treatment is applied to the sample before and after the annealing to ensure high-quality surface throughout the entire processing procedures. 26 In the end, each SIL contains multiple GeV color centers, and single quantum emitters can be selected via a combination of spatial mapping and resonant excitation thanks to a slight inhomogeneity of local strains around each GeV.

The sample is cooled down to 4.2 K and interrogated using a home-built confocal microscope, as shown in Fig. 1(a) (details in 23). When detecting resonance fluorescence from the GeV, the resonant laser scattering is suppressed via a cross polarization scheme at 30 dB extinction ratio. This is realized by adjusting the half wave-plate (HWP) and quarter wave-plate (QWP) in the collection path to tune the polarization of laser scattering perpendicular to the polarizer afterwards. When detecting phonon-side band (PSB) emission, a 650 ± 20 nm band-pass filter is placed in the collection path to reject the laser scattering

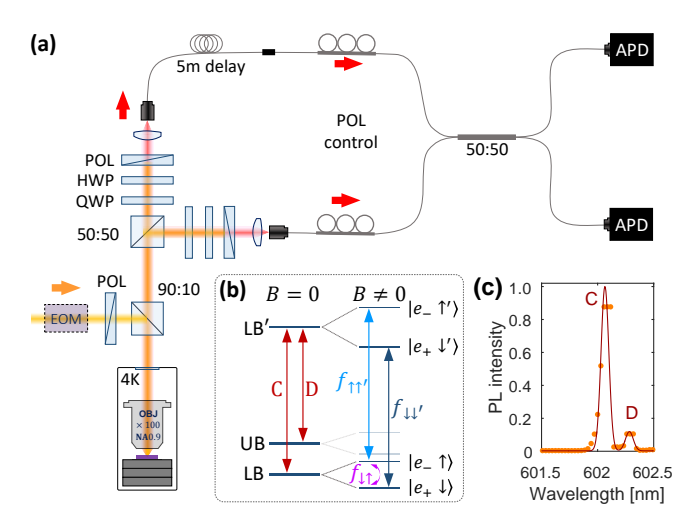
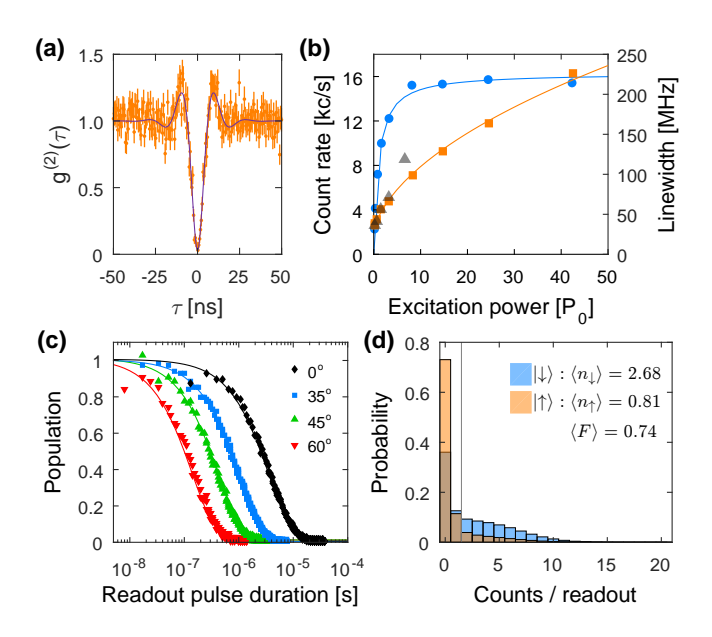


Figure 1: (a) Experiment setup. HWP: half wave-plate. QWP: quarter wave-plate. POL: polarizer. EOM: electro-optic modulator. APD: avalanche photodiode. (b) Energy levels of a GeV color center in diamond in zero and non-zero external magnetic field. The field lifts the double-degeneracy of the four orbitals, labeled as LB, UB, LB' and UB' (UB' is not shown) and reveals the spin degrees of freedom of the system including two cycling transitions $f_{\uparrow\uparrow}$ and $f_{\downarrow\downarrow}$ between LB and LB', and a flip-flop transition $f_{\uparrow\downarrow}$ in LB. LB: lower branch. UB: upper branch. Prime denotes the excited state. (c) Photoluminescence spectrum of GeVs at 4.2 K under 532 nm 0.46 mW excitation, monitored through a 600 \pm 7 nm band-pass filter. The solid line is a Gaussian fit, finding the ground orbital splitting of 180 GHz between LB and UB.

with a suppression ratio of > 70 dB.

When the GeV is illuminated with 532 nm non-resonant light, even though both excited orbitals are equally populated, the population in the upper branch (UB') immediately relaxes to the lower branch (LB') by emitting phonons [see Fig. 1(b)]. The lack of high-energy phonons (~1 THz) in diamond at 4 K allows for the accumulation of almost all population in LB' before any radiative decay takes place. ²⁷ This results in a two-line structure in the PL spectrum, ²⁸ corresponding to the decays from LB' to the double-degenerated ground orbitals LB and UB, as shown in Fig. 1(c). In fact, multiple GeVs are present in the excitation volume and contribute to the observed two-line structure. Thanks to the narrow emission linewidth and slight variations of local strain environment around each emitter, single GeVs can be addressed by employing resonant excitation, as shown by the wide-range photoluminescence excitation (PLE) spectrum in. ²³ We focus on the GeVs with bright and stable emission

for further studies. By monitoring the PSB emission from the resonantly addressed GeV, we are able to confirm the singleness of the photon source by measuring the second-order correlation function in Hanbury Brown-Twiss (HBT) configuration, ²⁹ typically observing a value $g^{(2)}(0) = 0.028 \pm 0.009$, as shown in Fig. 2(a).



(a) Second-order correlation function of PSB photons (650 \pm 20 nm) from a resonantly driven GeV. The solid line is a fit by solving a coherently driven 2-level system: $g^{(2)}(\tau) = 1 - \beta e^{-\eta \tau} [\cos(\nu \tau) + (\eta/\nu)\sin(\nu \tau)], \text{ with } \eta = (1/T_1 + 1/T_2)/2, \nu = 1/T_1 + 1/T_2$ $\sqrt{\Omega^2 - (1/T_1 - 1/T_2)^2/4}$. Here, $\beta = 0.972$ is the dip depth, $T_1 = 5.5$ ns and $T_2 = 7.1$ ns are the lifetime and coherence time of the excited state, and $\Omega = 0.57$ GHz is the Rabi frequency. (b) Count rate (blue circle) and linewidth (orange square for PSB, grey triangle for ZPL) extracted from a Lorentzian fit to the PLE spectra in Supporting Information. Solid curves are the 2-level model fitting, with the saturation power $P_0 = 6.1 \pm 0.7$ nW and coherence time $T_2 = 9.5 \pm 0.4$ ns. (c) $|\downarrow\rangle$ population during the readout pulse that addresses $f_{\downarrow\downarrow'}$ transition resonantly. Prior to the readout, the spin is initialized to $|\downarrow\rangle$ state by pumping $f_{\uparrow\uparrow}$ transition at 1.6 P₀. The magnetic field is held at 1.107 T for all measurements; only the direction varies. Solid lines are single exponential fits with time constants 3.8 μ s, 1.0 μ s, 0.4 μ s, and 0.15 μ s for 0°, 35°, 45°, and 60° orientated field with respect to the sample plane, respectively. (d) Photon statistics of single-shot readout when reading $|\downarrow\rangle$ (blue) or $|\uparrow\rangle$ (red) state in B = 1.107 T along 0°. $\langle n_{\uparrow} \rangle$ and $\langle n_{\downarrow} \rangle$ are the average readout photon numbers. $\langle \mathcal{F} \rangle$ is the average fidelity.

To evaluate the dephasing of these optical transitions, we conduct power-dependent PLE measurements on the GeV by collecting either PSB or ZPL emission. The increase of resonant excitation power broadens the PLE linewidth evidently and saturates the emission intensity

at $P_0 = 6.1$ nW, matching the predictions of a 2-level system, as shown in Fig. 2(b). Apart from the deviation of ZPL PLE linewidth at 6 P_0 , caused by the fluctuations of resonant laser scattering, the main difference is the 3 times stronger intensity for resonance fluorescence than the PSB emissions thanks to the 2:1 ZPL/PSB ratio and the finite PSB detection bandwidth (defined by the filter ~ 40 nm). Extrapolating the excitation power to 0 nW, we obtain an optical linewidth of 34 MHz, corresponding to a coherence time of $T_2 = 9.5$ ns. Considering the excited state lifetime T_1 of 5.5 ns, determined by time-resolved measurements, 23 we obtain $T_2/2T_1 = 0.86$, marking the Fourier-transform limited linewidth emission from a GeV. We confirm this narrow linewidth emission on several GeVs located in different SILs. 23 The generality of this excellent optical properties across the sample implies that our treatment of the diamond, including high-temperature annealing and acid cleaning, are beneficial to stabilize the local environment around GeV color centers.

According to the PL spectrum in Fig. 1(c), this GeV possesses a ground-state splitting of 180 GHz, which is 20 GHz greater than the intrinsic non-strained value of 160 GHz, ¹⁷ and can be categorized as a low-strain environment. Since moderate strains cannot dominate the spin-orbit coupling and the different coupling strengths give rise to different g-factors for the ground and excited states, ³¹ an external magnetic field thus is able to produce two spin-selective transitions, $f_{\downarrow\downarrow'}$ and $f_{\uparrow\uparrow'}$, as shown in Fig. 1(b). These spin conserving transitions are ideal for single-shot readout of spin states. Due to the different anisotropies of g tensors of the ground and excited states, the number of repetitive readout until a spin flip is field-orientation dependent, as shown in Fig. 2(c). Generally, a larger field misalignment from the symmetry axis of GeV induces a faster spin relaxation. Experimentally, we initialize the system to $|\downarrow\rangle$ state by pumping $f_{\uparrow\uparrow'}$ transition for 500 μ s followed by a 1 ms readout that addresses $f_{\downarrow\downarrow'}$ transition. When the magnetic field is closely aligned to the GeV symmetric axis, the spin can withstand a thousand times readout before experiencing a flip. By selecting an optimum readout window of 80 μ s and a threshold of 1.5 photons per readout, ²³ we achieve single-shot readout of $|\uparrow\rangle$ and $|\downarrow\rangle$ state with a fidelity of 63.9% and 84.5%, respectively, as

shown in Fig. 2(d). The final fidelity \mathcal{F} of readout, i.e., the average of the two, is 74.2%, limited by the spin pumping efficiency of initialization.²³

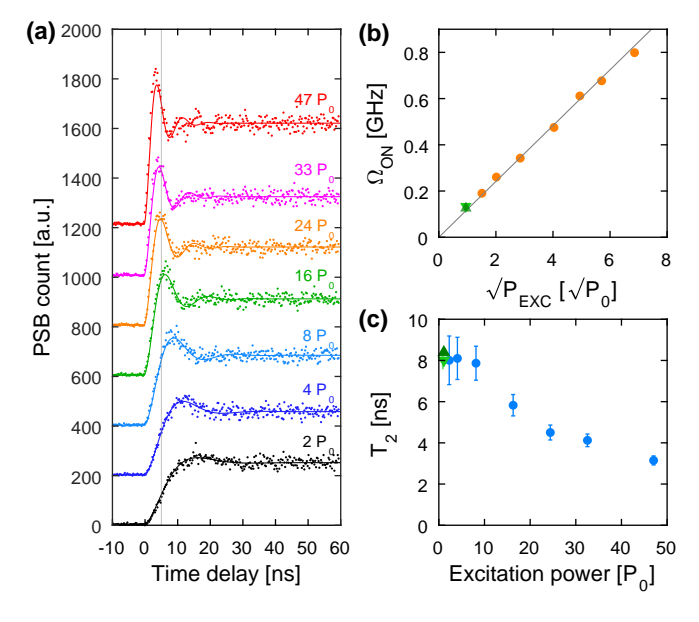


Figure 3: (a) Optical Rabi oscillations of the GeV under resonant excitations (vertical shifted for clarity). The solid lines are the fits by solving semi-classical 2-level master equation. ²³ The vertical grey line marks the 5-ns pulse width used for pulsed two-photon interference (TPI) experiment. (b) Rabi frequency $\Omega_{\rm ON}$ when the EOM switches on, following linearly over the square root of excitation power (grey). (c) Coherence time T_2 extracted from the Rabi oscillations in (a). The green upward and downward triangles in (b) and (c) are the parameters extracted from the continuous-wave TPI measurements.

To find the optical π -pulse of resonant excitation, we study the power-dependent timeresolved PL from the GeV by modulating the excitation beam with an electro-optic modulator (EOM), as shown in Fig. 3(a). We model the optically driven GeV as a two level system using the master equation with Lindblad terms that consider both spontaneous decay and pure dephasing. ²³ The extracted Rabi frequency Ω_{ON} (when the EOM switches on) increases linearly over the square root of the excitation power [Fig. 3(b)], while the coherence time T_2 drops monotonically from 8 ns to 3 ns as the excitation power increases from 2 P₀ to 50 P₀ [Fig. 3(c)]. We tentatively attribute the escalated dephasing to the laser-induced environmental fluctuations. ³² Two factors are considered for optimizing the pulse duration: a short pulse is needed to minimize the two-photon emission probability during the excitation period, while a long pulse is favored for laser suppression. We choose a pulse length close to the excited state lifetime with a power of 39 P_0 to realize the π -rotation of orbital populations.

Due to electron-phonon interactions, ²⁷ the PSB photons are distributed across a wide spectral range and are distinguishable in energy. Therefore, the coherent ZPL photons have to be used for TPI measurements. But the resonant laser scattering is not completely suppressed due to the finite suppression ratio, which can introduce a non-trivial impact on the photon statistics. We evaluate this influence by measuring HBT statistics of ZPL emissions from the GeV, as shown in Fig. 4(a). Firstly, the finite suppression ratio of cross polarization configuration results in a much shallower antibunching dip of 0.3 at $\tau = 0$ for CW excitation compared to the PSB detection as shown in Fig. 2(a). Secondly, the antibunching dip of pulsed excitation (which is 50 times stronger in excitation power compared to the CW driving) is about 0.05 and is less influenced by the laser photons. This may relate to the dark state of the GeV color center, which effectively reduces the signal-background ratio, ²³ leading to a rising of $q^{(2)}(0)$. Earlier studies show that the CW resonant driving can shelve the GeV emitter into a dark state via its excited state over a time scale of ms. 32 In pulsed excitation, however, each excitation sustains only a short period of time of 5 ns ($\sim T_1$) while the dwell time between two consecutive excitations is more than 5 T_1 . This waiting period is long enough for the GeV to relax back to its ground state via radiative decay, and prevents itself from being shelved to the dark state by the second excitation.

To perform TPI, we delay one emitted photon, and interfere two consecutive photons emitted from the same defect at the beam splitter. The delay δt is about 25 ns, achieved by adding an additional 5-meter-long optical fiber to one detection arm, as shown in Fig. 1(a). This delay is almost twice the coherence time of single photons from the GeV color center and ensures the vanishing probability of self field-field interference at the BS. By controlling the polarizations of the interfering photons, we conduct TPI measurements for both indistinguishable $[g_{\perp}^{(2)}(\tau)]$ and distinguishable $[g_{\perp}^{(2)}(\tau)]$ photons, as shown in Fig. 4(b). The deeper central dip of $g_{\parallel}^{(2)}(\tau)$ as compared to $g_{\perp}^{(2)}(\tau)$ reflects the TPI of indistinguishable photons,

imposed by the bosonic nature of photons.³³ The non-vanishing $g_{\parallel}^{(2)}(0)$, on the other hand, implies the imperfect experimental conditions including excitation laser leakage and dephasing of the photon source over time δt . We note that the instrument response function (IRF) here is at least one order of magnitude faster than the dip width of the correlation functions, thus playing a negligible role in data processing.

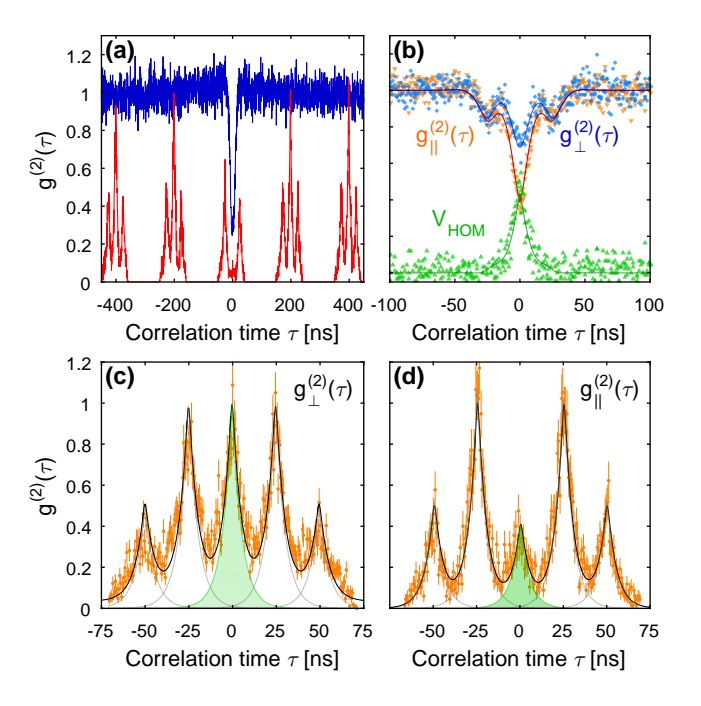


Figure 4: (a) Normalized HBT correlations of ZPL photons from the CW-driven (blue) or pulsed-driven (red) GeV, with resonant power 0.8 P_0 and 39 P_0 , respectively. The three correlation peaks in pulsed excitation correspond to the two consecutive excitations separated by δt . (b) CW TPI when detecting ZPL photons in aligned $(g_{\parallel}^{(2)}(\tau), \text{ orange})$ or orthogonal $(g_{\perp}^{(2)}(\tau), \text{ blue})$ polarizations. The solid lines are the fitting by solving 2-level master equation. V_{HOM} is the Hong-Ou-Mandel visibility following $1-g_{\parallel}^{(2)}(\tau)/g_{\perp}^{(2)}(\tau)$. (c-d) Pulsed TPI results measured in cross (c) or parallel (d) polarizations. The black curves are the sum of five exponential cusps (grey). The areas of the central shaded green cusp are used to evaluate the HOM visibility. See the main text for details.

The HOM visibility $V_{\text{HOM}}(\tau)$ is evaluated via $V_{\text{HOM}}(\tau) = (g_{\perp}^{(2)}(\tau) - g_{\parallel}^{(2)}(\tau))/g_{\perp}^{(2)}(\tau)$, as shown by the green triangles in Fig. 4(b). However, the value $V_{\text{HOM}}(0)$ strongly depends on the jittering of the detectors and a perfect detector with zero response time will always measure $V_{\text{HOM}}(0) = 0$ no matter how different the frequencies of two interfering photons are.³⁴ Thus, another figure-of-merit, the coalescence time window CTW= $\int d\tau V_{\text{HOM}}(\tau)$, ³⁵

is employed to quantify the indistinguishability. This value defines a time window beyond which no more deterministic coalescence of two photons can take place at the BS. Our data gives a CTW of 5.8 ns, close to the excited state lifetime T_1 of the GeV. Ideally, it should be about 2 T_1 for perfectly indistinguishable photons, whereas in our case, the dephasing $(T_2 < 2T_1)$ and the residual laser photons compromise this figure. We model the GeV system as a coherently driven 2-level emitter plus a resonant laser background to fit the measured results, 23 and find a Rabi frequency $\Omega = 0.13$ GHz and a coherence time T_2 of 8.4 ± 0.2 ns and 8.0 ± 0.4 ns for $g_{\parallel}^{(2)}(\tau)$ and $g_{\perp}^{(2)}(\tau)$, respectively. All these numbers are consistent with the earlier Rabi measurements, as shown by the green triangles in Fig. 3(b) and (c).

We also evaluate the indistinguishability of pulse-excitation generated single photons since these photons can be produced on demand. By matching the separation of two excitation pulses to the path difference of two detection arms, we observe five correlation peaks at the correlation time $\tau = -2\delta t$, $-\delta t$, 0, δt , and $2\delta t$, respectively, with an amplitude ratio of 1:2:2:2:1 if the photons are distinguishable, as shown in Fig. 4(c). After aligning the polarizations, the TPI reduces the coincidence count at τ =0, leading to an amplitude ratio of 1:2:x:2:1, as shown in Fig. 4(d). The incomplete vanishing of the central peak implies the distinguishable properties of interfering photons inherited from the photon source and the potential contamination from the residual laser photons. Phenomenologically, we fit each peak as a cusp of single exponential decay following $A \exp(-|\tau - t_0|/\tau_0)$, where τ_0 describes the time span of interfering photons and is shared among all ten peaks, and amplitude A represents the area of each peak that follows the ratio above. The HOM visibility can be evaluated via $V_{\text{HOM}} = (A_{\perp} - A_{\parallel})/A_{\perp} = 0.604 \pm 0.022$, with A_{\perp} and A_{\parallel} representing the areas of the central cusp (green shaded region) in Fig. 4(c) and (d), respectively, which is consistent with the fitting result based on a semiclassical model.²³

The current visibility is mainly limited by two factors: the non-lifetime-limited coherence of photons at high excitation powers and the finite laser suppression ratio. Since the dephasing of the GeV is caused by the fluctuations of surrounding environment, We has to, we can mask up the surrounding environment around the SILs to protect the local environment from damaged brough by ion implantations. Regarding the suppression, a few orders of magnitude improvement is possible ³⁶ if the sample vibrations can be restrained. ²³ Alternatively, switching to other nanostructures for collection enhancement, such as nanobeam photonic structure ³⁷ or nano pillars ³⁸ may also alleviate the issue. Despite the symmetry-protected optical transitions, we still observe spectral diffusions of GeVs over days, possibly caused by the second-order Stark effect and local strain fluctuations. ³⁹ One solution is to exploit Purcell effect of nanocavities to broaden the emission line to exceed the spectral diffusion. ⁴⁰ Alternatively, one can utilize strain tuning techniques to actively counter the spectral diffusion, provided a high-enough collection efficiency to enable transition frequency determination on a rate faster than the spectral diffusion. ^{41,42}

We demonstrate lifetime-limited linewidth emission from the GeV color center in diamond with $T_2/2T_1 \sim 0.86$. The enhanced collection efficiency of SIL microstructure allows for single-shot readout of spin states of the GeV color center with a fidelity of 74%, limited by the spin pumping efficiency of 80%. This can be improved by carefully aligning the magnetic field to the symmetric axis of the GeV. The two 25 ns-separated ZPL photons from a single GeV possess a coalescent time window of $\approx T_1$ under CW driving and a HOM visibility of $V_{\text{HOM}} = 0.604 \pm 0.022$ under pulsed excitation. The TPI performance is currently limited by the finite laser suppression of resonant laser and local strain fluctuations. Utilizing the strain tuning technique to feedback stabilize the optical transition frequency, it is possible to overcome these limitations.

Methods

The GeV color centers investigated in this work is generated via ion implantation in a Type-IIa electronic grade diamond substrate (Element Six). Before the implantation, the microstructures of solid-immersion lens (with a diameter of $\sim 5 \mu m$ and a height of 2.5 μm) were fabricated on the surface via focused ion beam etching. After fabrications, Ge ions

were implanted into the diamond with an energy of 10 MeV and a fluence of 10×10^{10} . The sample was then cleaned in hot Piranha Acid before completing a high-temperature annealing. More details in sample preparation can be found in Supporting Information.²³

The sample is placed in a dilution refrigerator (Bluefors LD250) for cryo measurements. The AMI 9-3T two-dimensional vector superconducting magnet allows arbitrary orientation of the magnetic field in YZ plane. We utilize a OPO SHG based tunable CW laser (Hubner C-wave) for resonantly driving of GeV color centers. For pulsed excitation, we pass the CW laser light through an EOM (Jenoptik) to obtain short laser pulses of a few nanosecond long. The PL of sample is collected with an objective of NA 0.9 before coupled into a singlemode fiber. The photons are registered by avalanche photodiode from Excelias for photon counting. The half-wave plate (HWP) and quarter-wave plate (QWP) in the collection paths are set to establish cross polarization scheme to eliminate the resonant laser scattering at an extinction ratio of 30 dB, while the fiber-based polarization control in each arm is used to generate cross or parallel polarizations between the two interfering photons at the second BS. When phonon-side band (PSB) detection is needed, a 650 ± 20 nm band-pass filter is placed in collection path (between the two BS cubes) to reject the laser reflection at 70 dB suppression. We note that a low-power green laser is always introduced to the GeV during resonant excitation. It is needed to stabilize the GeV's charge state, without which no resonance fluorescence of GeV can be detected. We stress that the laser power (of the green laser) is so weak that no fluorescence can be induced from the GeV by itself. The only function it serves is to tune the local Fermi level in favor of -1 charge state, as explained in earlier studies.³²

Acknowledgement

We acknowledge Singapore National Research foundation through QEP grant (NRF2021-QEP2-01-P02, NRF2021-QEP2-03-P01, 2019-0643 (QEP-P2) and 2019-1321 (QEP-P3)) and

Singapore Ministry of Education (MOE2016-T3-1-006 (S)), the Australian Research council (via CE200100010), the Asian Office of Aerospace Research and Development grant FA2386-17-1-4064.

Competing interests: The authors declare no competing financial interest.

References

- (1) Flamini, F.; Spagnolo, N.; Sciarrino, F. Photonic quantum information processing: a review. Reports on Progress in Physics 2018, 82, 016001.
- (2) Slussarenko, S.; Pryde, G. J. Photonic quantum information processing: A concise review. *Applied Physics Reviews* **2019**, *6*, 041303.
- (3) Pirandola, S.; Eisert, J.; Weedbrook, C.; Furusawa, A.; Braunstein, S. L. Advances in quantum teleportation. *Nature Photonics* **2015**, *9*, 641–652.
- (4) Kimble, H. J. The quantum internet. *Nature* **2008**, 453, 1023–1030.
- (5) Pan, J.-W.; Chen, Z.-B.; Lu, C.-Y.; Weinfurter, H.; Zeilinger, A.; Żukowski, M. Multiphoton entanglement and interferometry. *Reviews of Modern Physics* **2012**, *84*, 777–838.
- (6) Reiserer, A.; Rempe, G. Cavity-based quantum networks with single atoms and optical photons. Reviews of Modern Physics 2015, 87, 1379–1418, Publisher: American Physical Society.
- (7) Meraner, M.; Mazloom, A.; Krutyanskiy, V.; Krcmarsky, V.; Schupp, J.; Fioretto, D. A.; Sekatski, P.; Northup, T. E.; Sangouard, N.; Lanyon, B. P. Indistinguishable photons from a trapped-ion quantum network node. *Physical Review A* 2020, 102, 052614.
- (8) Schimpf, C.; Reindl, M.; Basso Basset, F.; Jöns, K. D.; Trotta, R.; Rastelli, A. Quantum

- dots as potential sources of strongly entangled photons: Perspectives and challenges for applications in quantum networks. *Applied Physics Letters* **2021**, *118*, 100502.
- (9) Awschalom, D. D.; Hanson, R.; Wrachtrup, J.; Zhou, B. B. Quantum technologies with optically interfaced solid-state spins. *Nature Photonics* **2018**, *12*, 516–527.
- (10) Hepp, C.; Müller, T.; Waselowski, V.; Becker, J. N.; Pingault, B.; Sternschulte, H.; Steinmüller-Nethl, D.; Gali, A.; Maze, J. R.; Atatüre, M.; Becher, C. Electronic Structure of the Silicon Vacancy Color Center in Diamond. *Phys. Rev. Lett.* 2014, 112, 036405.
- (11) Castelletto, S.; Rosa, L.; Blackledge, J.; Al Abri, M. Z.; Boretti, A. Advances in diamond nanofabrication for ultrasensitive devices. *Microsystems & Nanoengineering* **2017**, *3*, 1–16.
- (12) Pelucchi, E. et al. The potential and global outlook of integrated photonics for quantum technologies. *Nature Reviews Physics* **2021**, 1–15.
- (13) Wan, N. H.; Lu, T.-J.; Chen, K. C.; Walsh, M. P.; Trusheim, M. E.; De Santis, L.; Bersin, E. A.; Harris, I. B.; Mouradian, S. L.; Christen, I. R.; Bielejec, E. S.; Englund, D. Large-scale integration of artificial atoms in hybrid photonic circuits. *Nature* **2020**, *583*, 226–231.
- (14) Siyushev, P. et al. Optical and microwave control of germanium-vacancy center spins in diamond. *Physical Review B* **2017**, *96*, 081201.
- (15) Iwasaki, T. et al. Germanium-Vacancy Single Color Centers in Diamond. *Scientific Reports* **2015**, *5*, 12882.
- (16) Rogers, L. J.; Jahnke, K. D.; Teraji, T.; Marseglia, L.; Müller, C.; Naydenov, B.; Schauffert, H.; Kranz, C.; Isoya, J.; McGuinness, L. P.; Jelezko, F. Multiple intrinsically

- identical single-photon emitters in the solid state. *Nature Communications* **2014**, *5*, 4739.
- (17) Bhaskar, M.; Sukachev, D.; Sipahigil, A.; Evans, R.; Burek, M.; Nguyen, C.; Rogers, L.; Siyushev, P.; Metsch, M.; Park, H.; Jelezko, F.; Lončar, M.; Lukin, M. Quantum Nonlinear Optics with a Germanium-Vacancy Color Center in a Nanoscale Diamond Waveguide. *Physical Review Letters* 2017, 118, 223603.
- (18) Palyanov, Y. N.; Kupriyanov, I. N.; Borzdov, Y. M.; Surovtsev, N. V. Germanium: a new catalyst for diamond synthesis and a new optically active impurity in diamond. *Scientific Reports* 2015, 5, 14789.
- (19) Sipahigil, A.; Jahnke, K.; Rogers, L.; Teraji, T.; Isoya, J.; Zibrov, A.; Jelezko, F.; Lukin, M. Indistinguishable Photons from Separated Silicon-Vacancy Centers in Diamond. *Physical Review Letters* 2014, 113, 113602.
- (20) Hong, C. K.; Ou, Z. Y.; Mandel, L. Measurement of subpicosecond time intervals between two photons by interference. *Physical Review Letters* **1987**, *59*, 2044–2046.
- (21) Evans, R. E.; Sipahigil, A.; Sukachev, D. D.; Zibrov, A. S.; Lukin, M. D. Narrow-Linewidth Homogeneous Optical Emitters in Diamond Nanostructures via Silicon Ion Implantation. *Physical Review Applied* 2016, 5, 044010.
- (22) Chu, Y. et al. Coherent Optical Transitions in Implanted Nitrogen Vacancy Centers.

 Nano Letters 2014, 14, 1982–1986.
- (23) Supporting Information for "Quantum interference of resonance fluorescence from Germanium-vacancy color centers in diamond". See Supporting Information, which includes details on sample fabrications, optical measurements, resonance photoluminescence, single-shot readout of spin states, Rabi oscillations, and two-photon interference.

- (24) Jamali, M.; Gerhardt, I.; Rezai, M.; Frenner, K.; Fedder, H.; Wrachtrup, J. Microscopic diamond solid-immersion-lenses fabricated around single defect centers by focused ion beam milling. *Review of Scientific Instruments* **2014**, *85*, 123703.
- (25) Hadden, J. P.; Harrison, J. P.; Stanley-Clarke, A. C.; Marseglia, L.; Ho, Y.-L. D.; Patton, B. R.; O'Brien, J. L.; Rarity, J. G. Strongly enhanced photon collection from diamond defect centers under microfabricated integrated solid immersion lenses. *Applied Physics Letters* 2010, 97, 241901.
- (26) Sangtawesin, S. et al. Origins of Diamond Surface Noise Probed by Correlating Single-Spin Measurements with Surface Spectroscopy. *Physical Review X* **2019**, *9*, 031052.
- (27) Jahnke, K. D.; Sipahigil, A.; Binder, J. M.; Doherty, M. W.; Metsch, M.; Rogers, L. J.; Manson, N. B.; Lukin, M. D.; Jelezko, F. Electron-phonon processes of the silicon-vacancy centre in diamond. New Journal of Physics 2015, 17, 043011.
- (28) Ekimov, E. A.; Lyapin, S. G.; Boldyrev, K. N.; Kondrin, M. V.; Khmelnitskiy, R.; Gavva, V. A.; Kotereva, T. V.; Popova, M. N. Germanium-vacancy color center in isotopically enriched diamonds synthesized at high pressures. *JETP Letters* 2015, 102, 701–706.
- (29) Hanbury Brown, R.; Twiss, R. Q. A Test of a New Type of Stellar Interferometer on Sirius. *Nature* **1956**, *178*, 1046–1048.
- (30) Flagg, E. B.; Muller, A.; Robertson, J.; Founta, S.; Deppe, D.; Xiao, M.; Ma, W.; Salamo, G.; Shih, C.-K. Resonantly driven coherent oscillations in a solid-state quantum emitter. *Nature Physics* **2009**, *5*, 203–207.
- (31) Nguyen, C. T.; Sukachev, D. D.; Bhaskar, M. K.; Machielse, B.; Levonian, D. S.; Knall, E. N.; Stroganov, P.; Chia, C.; Burek, M. J.; Riedinger, R.; Park, H.; Lončar, M.; Lukin, M. D. An integrated nanophotonic quantum register based on silicon-vacancy spins in diamond. *Physical Review B* 2019, 100, 165428.

- (32) Chen, D.; Mu, Z.; Zhou, Y.; Fröch, J. E.; Rasmit, A.; Diederichs, C.; Zheludev, N.; Aharonovich, I.; Gao, W.-b. Optical Gating of Resonance Fluorescence from a Single Germanium Vacancy Color Center in Diamond. *Physical Review Letters* 2019, 123, 033602.
- (33) Fearn, H.; Loudon, R. Theory of two-photon interference. JOSA B 1989, 6, 917–927.
- (34) Koong, Z.; Scerri, D.; Rambach, M.; Santana, T.; Park, S.; Song, J.; Gauger, E.; Gerardot, B. Fundamental Limits to Coherent Photon Generation with Solid-State Atomlike Transitions. *Physical Review Letters* **2019**, *123*, 167402.
- (35) Proux, R.; Maragkou, M.; Baudin, E.; Voisin, C.; Roussignol, P.; Diederichs, C. Measuring the Photon Coalescence Time Window in the Continuous-Wave Regime for Resonantly Driven Semiconductor Quantum Dots. *Physical Review Letters* 2015, 114, 067401.
- (36) Kuhlmann, A. V.; Houel, J.; Brunner, D.; Ludwig, A.; Reuter, D.; Wieck, A. D.; Warburton, R. J. A dark-field microscope for background-free detection of resonance fluorescence from single semiconductor quantum dots operating in a set-and-forget mode. Review of Scientific Instruments 2013, 84, 073905.
- (37) Burek, M. J.; Chu, Y.; Liddy, M. S. Z.; Patel, P.; Rochman, J.; Meesala, S.; Hong, W.; Quan, Q.; Lukin, M. D.; Lončar, M. High quality-factor optical nanocavities in bulk single-crystal diamond. *Nature Communications* **2014**, *5*, 1–7.
- (38) Zhang, J. L.; Lagoudakis, K. G.; Tzeng, Y.-K.; Dory, C.; Radulaski, M.; Kelaita, Y.; Fischer, K. A.; Sun, S.; Shen, Z.-X.; Melosh, N. A.; Chu, S.; Vučković, J. Complete coherent control of silicon vacancies in diamond nanopillars containing single defect centers. *Optica* **2017**, 4, 1317–1321.
- (39) Meesala, S. et al. Strain engineering of the silicon-vacancy center in diamond. *Physical Review B* **2018**, *97*, 205444.

- (40) Evans, R. E.; Bhaskar, M. K.; Sukachev, D. D.; Nguyen, C. T.; Sipahigil, A.; Burek, M. J.; Machielse, B.; Zhang, G. H.; Zibrov, A. S.; Bielejec, E.; Park, H.; Lončar, M.; Lukin, M. D. Photon-mediated interactions between quantum emitters in a diamond nanocavity. *Science* 2018, eaau4691.
- (41) Machielse, B. et al. Quantum Interference of Electromechanically Stabilized Emitters in Nanophotonic Devices. *Physical Review X* **2019**, *9*, 031022.
- (42) Sohn, Y.-I. et al. Controlling the coherence of a diamond spin qubit through its strain environment. *Nature Communications* **2018**, *9*, 1–6.